ACS Catalysis

Research Article

pubs.acs.org/acscatalysis

Bioinspired Iron Sulfide Nanoparticles for Cheap and Long-Lived Electrocatalytic Molecular Hydrogen Evolution in Neutral Water

Carlo Di Giovanni,[†] Wei-An Wang,[‡] Sophie Nowak,[‡] Jean-Marc Grenèche,[§] Hélène Lecoq,[‡] Ludovic Mouton,[‡] Marion Giraud,*[,‡] and Cédric Tard*[,†]

[†]Laboratoire d'Électrochimie Moléculaire, UMR 7591 CNRS, Université Paris Diderot, Sorbonne Paris Cité, 15 rue Jean-Antoine de Baïf, F-75205 Paris Cedex 13, France

[‡]Laboratoire ITODYS, UMR 7086 CNRS, Université Paris Diderot, Sorbonne Paris Cité, 15 rue Jean-Antoine de Baïf, F-75205 Paris Cedex 13, France

[§]Institut des Molécules et Matériaux du Mans, IMMM, UMR 6283 CNRS, Université du Maine, Avenue Olivier Messiaen, F-72085 Le Mans Cedex 9, France

Supporting Information

ABSTRACT: Alternative materials to platinum-based catalysts are required to produce molecular hydrogen from water at low overpotentials. Transition-metal chalcogenide catalysts have attracted significant interest over the past few years because of their activity toward proton reduction and their relative abundance compared with platinum. We report the synthesis and characterization of a new type of iron sulfide (FeS, pyrrhotite) nanoparticles prepared via a solvothermal route. This material can achieve electrocatalysis for molecular hydrogen evolution with no structural decomposition or activity decrease for at least 6 days at a mild overpotential in neutral water at room temperature.

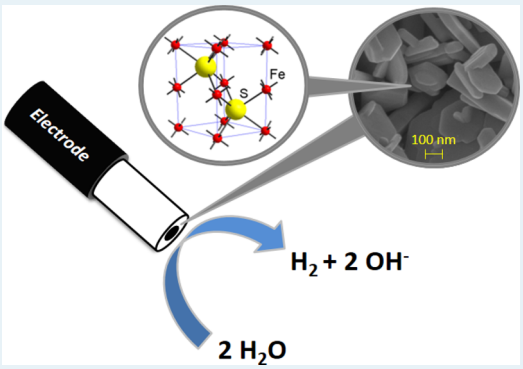

KEYWORDS: *hydrogen evolution reaction, iron sulfide nanoparticles, electrocatalysis, nanoparticle Mössbauer spectroscopy, electrode modification*

1. INTRODUCTION

Environmental and economic factors require a drastic change in energy production. Replacing fossil fuels by renewable and sustainable energy sources is an absolute necessity in order to face contemporary energy challenges. Molecular hydrogen is currently at the forefront for the prospect of new energy vectors as a way to store energy in chemical bonds. Its clean, cold combustion in fuel cells[1] or its production in water electrolyzers will require the replacement of noble-metal catalysts such as platinum and its alloys by earth-abundant catalysts for proton reduction into dihydrogen if worldwide use of hydrogen is considered.

Inspiration can be found in microorganisms and algae, where hydrogenase metalloenzymes are capable of reversibly converting protons into molecular hydrogen.[2] The active sites of these enzymes are made of Fe/S or Fe/Ni/S core clusters, and molecular hydrogen can be evolved at turnover frequencies as high as 9000 moles of H_2 per mole of hydrogenase per second in water at pH 7 and 30 °C.[3] Attempts to implement these enzymes onto electrodes have been made, but major practical drawbacks of these natural systems arise from their high oxygen sensitivity, their bulkiness (which limits the number of catalysts per unit of surface area), and the difficulty of producing high amounts of material for industrial purposes.[4] Despite numerous examples and attractive properties, such as their oxygen stability and solubility in different media, hydrogenase biomimetic synthetic molecular electrocatalysts, in solution or grafted onto an electrode, present poor to moderate activity toward molecular hydrogen evolution or uptake reactions.[5,6] Interestingly, it has been demonstrated that cubane-type Fe_4S_4 clusters can reduce protons into dihydrogen from weak organic acids,[7] but the poor stability of such molecules toward water and dioxygen is still problematic when considering these systems as potential efficient catalysts. It is worth noting that these molecular Fe_4S_4 clusters can be stabilized within porous chalcogenide frameworks and that such systems show activity for homogeneous electrocatalysis and photocatalysis for dihydrogen evolution and carbon dioxide reduction.[8−10]

Non-precious-metal catalysts operating at low overpotentials and high current densities under mild conditions (ca. pH 7, 1 atm, room temperature) that would compete with natural enzymes or platinum itself are scarce. Recently, long-lived and cheap coordination complexes that can homogenously reduce protons to molecular hydrogen in neutral aqueous media have

Received: December 9, 2013
Revised: January 14, 2014
Published: January 27, 2014

been prepared[11] using molybdenum,[12] cobalt,[13−15] or nickel[16,17] as metal centers. Furthermore, molybdenum sulfide electrocatalysts, in the form of nanocrystals,[18] amorphous electropolymerized films,[19,20] molecular complexes,[21] or amorphous particles,[22] or transition-metal alloys of nickel−molybdenum,[23,24] cobalt sulfide,[25] and iron[26] or nickel[27] phosphides have also been reported for their high activity toward molecular hydrogen evolution in acidic or neutral water at relatively low overpotentials and represent a very promising way to replace noble-metal catalysts. Therefore, we can think that stabilization of other types of transition-metal chalcogenide moieties within nanosystem assemblies could allow the preparation of cheap and sustainable bioinspired catalysts.

Given the ubiquity of iron sulfide minerals in nature, such as pyrite FeS_2, which is the most abundant mineral on the Earth's surface,[28] we decided to study the electrocatalytic properties of iron sulfide nanoparticles that can be synthesized easily and rapidly on a gram scale from an abundant and cheap precursor. Herein we report the preparation of air-stable pyrrhotite-type FeS nanoparticles dispersed in Nafion films, which exhibit molecular hydrogen evolution in neutral water at room temperature with catalytic stability exceeding 6 days of electrolysis.

2. RESULTS AND DISCUSSION

2.1. Synthesis and Characterization of Nanoparticles. The synthesis of pyrrhotite FeS nanoparticles was performed using a single precursor source, $Fe_2S_2(CO)_6$,[29,30] which decomposes in octylamine under solvothermal conditions at 230 °C. This simple and rapid method allows us to prepare nanoparticles in >80% yield. The chemical composition of the prepared powder was evaluated by energy-dispersive X-ray (EDX) measurements, which indicated that the powder mainly contained Fe and S atoms and corresponded to a 1:1 Fe/S stoichiometry (Figure S3 and Table S1 in the Supporting Information). The organic content of the powder, estimated via thermogravimetric analysis (TGA) measurements under air, was found to be negligible.

As displayed in Figure 1, the X-ray diffraction (XRD) pattern, which can be fully indexed in a pure pyrrhotite phase ($P6_3/mmc$ space group), reveals that the particles are crystalline. Refinement of the lattice parameters led to the values a = 3.450 Å and c = 5.770 Å, in good agreement with the values obtained for another synthetic pyrrhotite, $Fe_{1-0.125x}S$ ($0 \le x \le 1$), which has the NiAs structure.[31] They are rather close to those of $Fe_{0.921}S$ (ICSD 98-016-8077) in that study,[31] but since atomic positions and occupancies were not refined (only strain was refined through the "arbitrary texture" option of the MAUD software), one cannot conclude at this stage that this sample is exactly the same and possesses this refined stoichiometry. The mean crystallite size was estimated to be about 100 nm, but the refinement showed that the crystallites are anisotropic (Figure S6 and Table S2 in the Supporting Information).

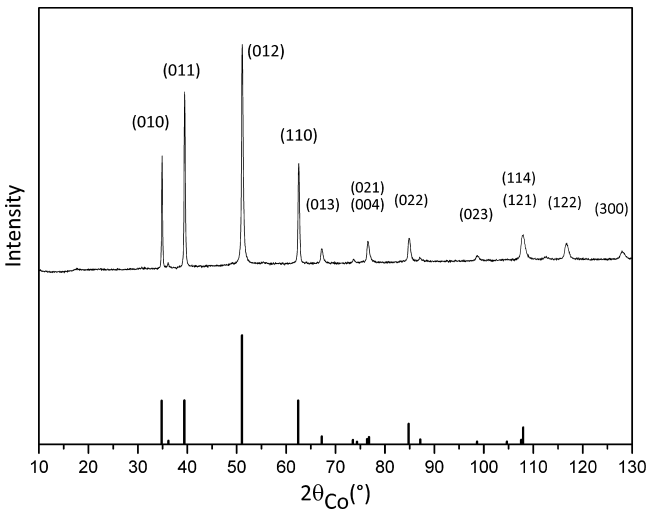

Figure 1. XRD pattern of FeS nanoparticles. The vertical bars represent the theoretical pattern for pyrrhotite $Fe_{0.921}S$ (ICSD 98-016-8077).[31]

The transmission electron microscopy (TEM) image (Figure 2 left) provides a 2D representation of the nanoparticles. The black powder recovered by centrifugation consists of hexagonally shaped nanoparticles that are polydispersed with sizes ranging from 50 to 500 nm. The size range values are close to the average coherent diffraction domain obtained by XRD (using the Debye−Scherrer law), suggesting that the particles are mostly single crystals. The selective-area electron diffraction (SAED) pattern on a single particle (Figure 3) shows a monocrystalline-particle diffraction pattern with sixfold symmetry, which is expected for a crystalline hexagonal array observed along the ⟨001⟩ zone axis. The scanning electron microscopy (SEM) image (Figure 2 right) reveals that the particles have a faceted platelet morphology with aspect ratios as low as 1/10 and confirms both the size range and the polydispersity of the sample observed by TEM. It also supports the very low content of organic matter in the sample.

In order to improve the structural characterization of our sample, we decided to use ^{57}Fe Mössbauer spectrometry, which is a sensitive tool for probing the local chemical environment, to bring information complementary to that of XRD. Indeed, the Mössbauer spectra recorded at both 300 and 77 K clearly exhibit a magnetic hyperfine structure with broadened lines (Figure 4).

The modeling procedure involved a discrete series of magnetic sextets with isomer shift values ranging from 0.68 to 0.78 mm/s and from 0.78 to 0.88 mm/s and hyperfine field values ranging from 23 to 31 T and from 25 to 35 T at 300 and 77 K, respectively, with rather low values of the quadrupole shift. As it was established above by X-ray diffraction that the sample is well-crystalline, the broadened lines should result from local chemical disorder in the environment of the Fe nuclei and a lack of stoichiometry. The mean values listed in Table 1 can be compared with those in the literature;[32] the present results allow us a priori to conclude that the Fe species belong to $Fe_{1-x}S$ sulfides, close to a S-deficient disordered pyrrhotite.

2.2. Electrochemical Studies and Stability of the Coated Electrode. Catalyst ink was prepared using a Nafion dispersion and FeS nanoparticles to evaluate the catalytic activity toward molecular hydrogen evolution. Vitreous carbon rotating disk electrodes (RDEs) were coated with FeS nanoparticles dispersed in Nafion and aged for 12 h at 100 °C in an oven. Analysis of a coated electrode film by SEM showed a rather dense and uniform film with a thickness estimated to be around 40 nm (Figure 5).

Under an argon atmosphere, cyclic voltammetry in 0.1 mol/L potassium phosphate (pH 7.0) exhibited a sharp rise in current from ca. −0.8 vs NHE (Figure 6). Some small bubbles evolved from the surface of the coated electrode, and from gas

dx.doi.org/10.1021/cs4011698 | ACS Catal. 2014, 4, 681−687

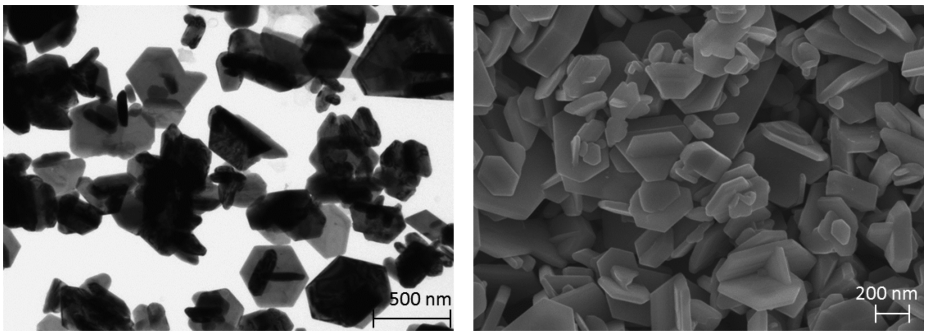

Figure 2. (left) TEM and (right) SEM images of FeS nanoparticles.

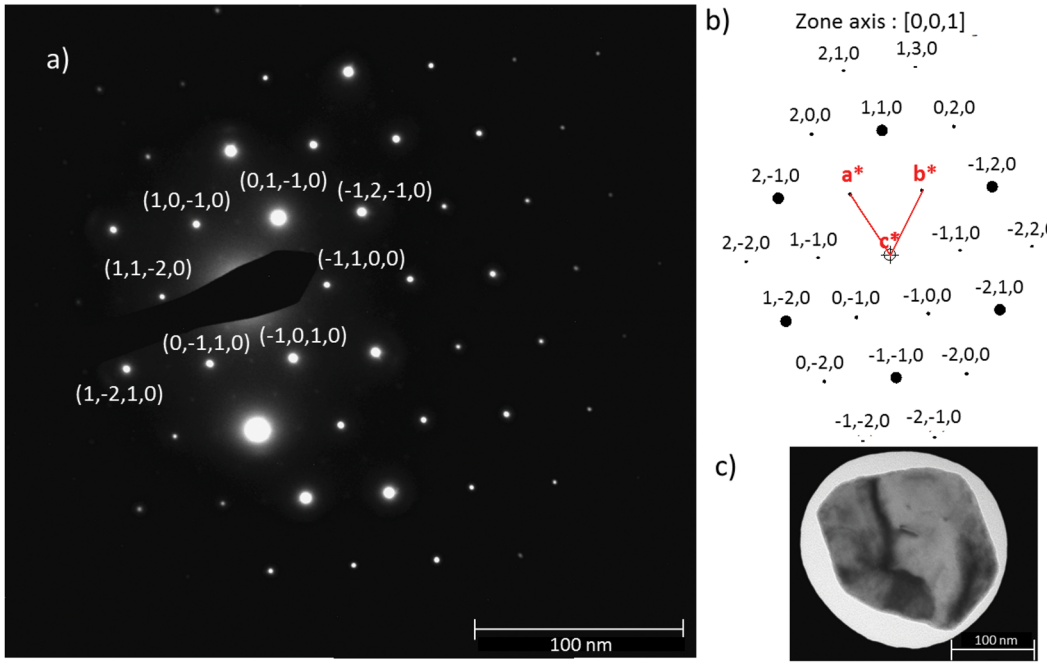

Figure 3. (a) SAED pattern along the ⟨001⟩ axis on the single particle shown in (c). (b) Theoretical pattern along this axis obtained with the Carine software.

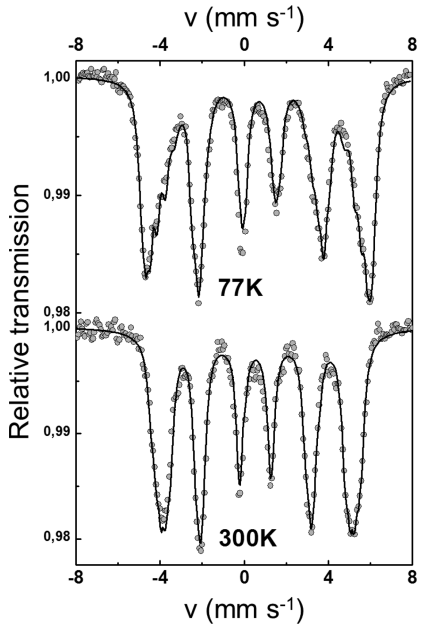

Figure 4. Mössbauer spectra recorded at 300 and 77 K.

Table 1. Mean Values of the Hyperfine Parameters Characteristic of the Prepared $Fe_{1-x}S$ Nanoparticles and Other Iron Sulfide Materials from the Literature

formula	T (K)	δ (mm/s)[a]	2ε (mm/s)[a]	B_{hf} (T)[b]	ref
$Fe_{1-x}S$	300	0.74	0.08	23.5	this work
FeS	300	0.7−0.9	−0.3	30−32	32
$Fe_{11}S_{12}$	300	0.55	0.05	22.0−23.5	32
$Fe_{10}S_{11}$	300	0.55	0.05	25.5−26.5	32
Fe_9S_{10}	300	0.55	0.10	27.5−31.5	32
Fe_7S_8	300	0.77	0.08	22.9	32
		0.79	0.03	26.7	
		0.79	0.15	31.1	
		0.81	−0.09	34.5	
$Fe_{1-x}S$	77	0.84	−0.02	30.7	this work

[a]Uncertainty = ±0.02 mm/s. [b]Uncertainty = ±0.5 T.

chromatography analysis we determined that this current enhancement was due to molecular hydrogen evolution. On the reverse scan we observed two oxidation peaks at −0.50 and −0.42 vs NHE, probably due to oxidation of hydride or dihydrogen species trapped at the surface of the catalytic film, but no further characterizations were performed. The coated

dx.doi.org/10.1021/cs4011698 | ACS Catal. 2014, 4, 681−687

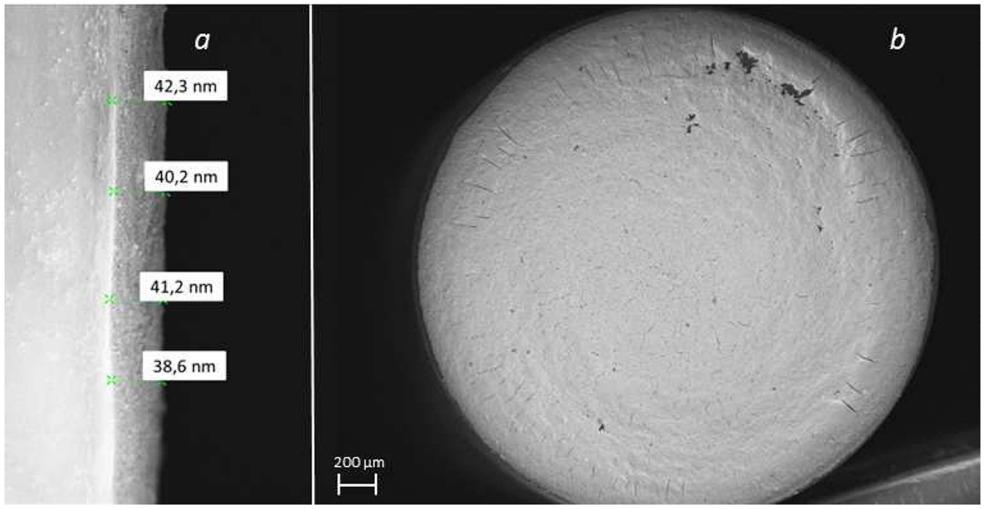

Figure 5. SEM images of an FeS nanoparticle/Nafion-coated rotating disk electrode: (a) side view; (b) top view.

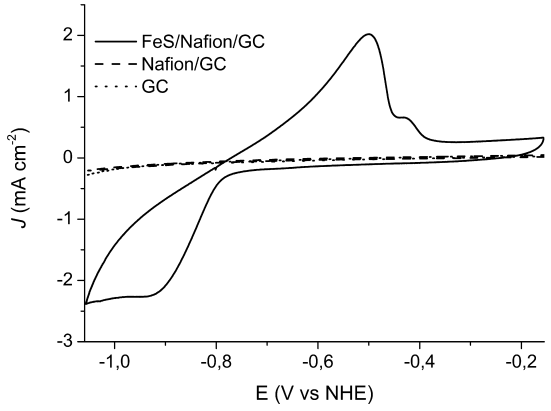

Figure 6. Cyclic voltammograms of FeS nanoparticles dispersed in Nafion on a rotating disk electrode (solid line), a Nafion-coated electrode (dashed line), and a bare electrode (dotted line). Voltammograms were recorded in 0.1 mol/L potassium phosphate buffer at pH 7.0 and 20 °C (scan rate 0.1 V/s; rotation rate 4000 rpm; scan number 10).

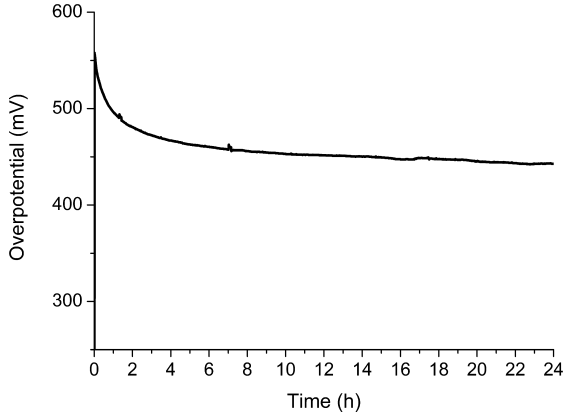

Figure 7. Galvanostatic control experiment on an electrode functionalized with FeS nanoparticles dispersed in Nafion (overpotential = | applied potential + 0.059 × pH| vs NHE). The experiment was performed on a rotating disk electrode in 0.1 mol/L potassium phosphate buffer at pH 7.0 and 20 °C (I = 50 μA; rotation rate 4000 rpm). No quantifiable pH variation during the experiment was observed.

electrodes were found to be stable for electrochemical studies for more than 6 months with no particular storage care.

The stability of the modified electrode was investigated over 24 h by a galvanostatic experiment at a current density of J = 0.7 mA cm^{-2} (I = 50 μA) at pH 7.0 (Figure 7). The decrease in overpotential observed during the first 24 h indicates a rise in the activity of the film toward H_2 generation, likely due to some modifications of the surface state of the catalyst. The overpotential then decreases slightly over the course of the experiment. The small spikes detected on the curve are due to the formation of small H_2 bubbles at the surface of the coated electrode.

To determine the dependence of the catalytic activity and film stability on pH, small amounts of concentrated HCl or NaOH were added under an argon atmosphere to a 0.1 mol/L buffered solution at pH 7.0 in order to vary the pH from 6.0 to 8.0. Higher catalytic activity (in terms of current density) was noted at lower pH. On the contrary, under basic conditions a strong decrease in the current was observed. It is worth mentioning that the pH changes did not produce irreversible alterations of the film, as the initial current density was fully recovered by restoring the initial pH 7.0 conditions (Figure 8).

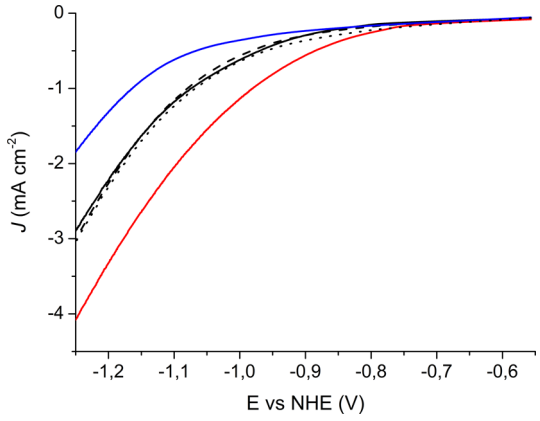

Figure 8. Linear sweep voltammetry of FeS nanoparticles dispersed in Nafion. Voltammograms were recorded on a rotating disk electrode in 0.1 mol/L potassium phosphate buffer at pH 6.0, 7.0, and 8.0 at 20 °C (scan rate 0.01 V/s; rotation rate 4000 rpm). Initial pH 7.0 conditions (solid black line); pH 6.0 (red line); pH 7.0 restored conditions from pH 6.0 (dashed line); pH 8.0 (blue line); pH 7.0 restored conditions from pH 8.0 (dotted line).

dx.doi.org/10.1021/cs4011698 | ACS Catal. 2014, 4, 681−687

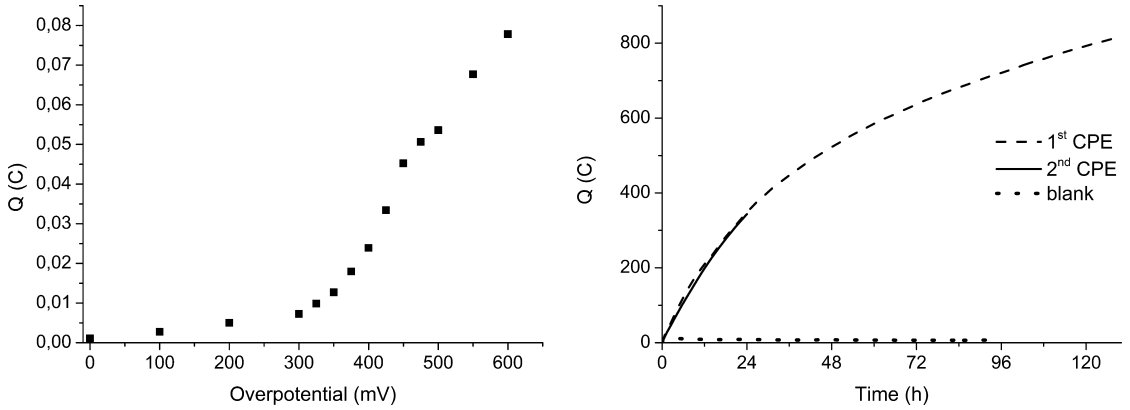

Figure 9. (left) Controlled-potential electrolysis of FeS nanoparticles in 0.1 mol/L potassium phosphate buffer at pH 7.0. (right) First (dashed line) and second (solid line) bulk electrolyses at an overpotential of 350 mV (−0.763 V vs NHE) in 1 mol/L potassium phosphate buffer at pH 7.0, showing a buildup of charge (Q) vs time [$Q = f(t)$] for the cell with and without (dotted line) FeS nanoparticles.

2.3. Controlled-Potential Electrolysis. Long-duration controlled-potential electrolysis (CPE) was performed to assess the durability and robustness of the FeS nanoparticle-coated electrode. Figure 9 (left) shows the amount of charge measured at different overpotentials (η = lapplied potential + 0.059 × pHl vs NHE) at pH 7.0 after subtraction of the contribution from the blank solution. Low current densities were observed at low overpotentials, and a sharp increase arises from 325 mV. To estimate the Faradaic efficiency for the H_2 production, CPE was performed in a 1 mol/L phosphate buffer solution at pH 7.0 over 5 days at η = 350 mV (−0.763 V vs NHE) (Figure 9 right, dashed line). Quantitative (≥0.99) Faradaic yield for molecular hydrogen evolution was confirmed by gas chromatography analysis as well as by volumetric measurements (Figure S8 in the Supporting Information). The slight decrease in the slope of the Q versus time curve is due to the pH increase of 0.3 unit caused by proton consumption. To further investigate this point, the crucible coated with the FeS nanoparticles was refilled with a fresh solution of 1 mol/L phosphate buffer at pH 7.0, and an identical Q versus time profile was obtained over a 1 day CPE under the same experimental conditions (Figure 9 right, solid line). Again, an almost quantitative Faradaic yield (≥0.98) was obtained for H_2 generation, outlining the remarkable stability of such nanoparticles over the course of catalysis. No particular care in storage of the catalyst or pre-degassing of the phosphate buffer solution was required, demonstrating the long-term stability of this material. After these 6 days of electrolysis, no major structural changes in the electrolyzed catalyst were observed by XRD (Figures S5–S7 in the Supporting Information), and the morphology of the FeS nanoparticles was also found to be unchanged (Figure S2 in the Supporting Information).

Comparison of different solid-state catalysts is a challenging task because of differences in the electrode preparation (coating vs electrodeposition) and the amount of material loaded onto the electrode. A rough comparison can be envisaged by measuring polarization curves and extracting the current density at an overpotential of 0 V (J_0) and the slope of this curve.[25] A measure of the catalytic activity of FeS nanoparticles was extrapolated from polarization curves in neutral water and compared with those of related solid-state catalysts for hydrogen evolution (Figure 10 and Table 2). A linear increase in log J was found in the overpotential range from 350 to 450 mV. At a given current density of J = 0.18 mA cm^{-2} (log J = −3.75), the overpotential of our material is shifted positively

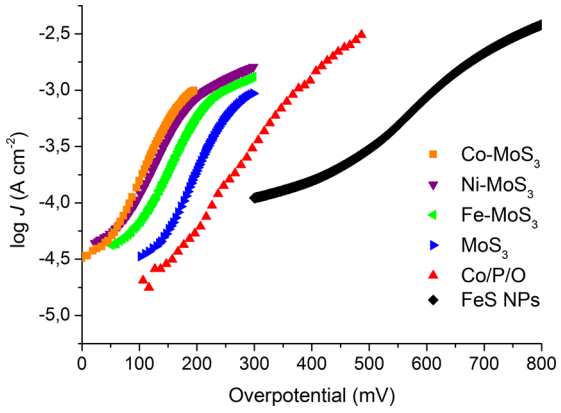

Figure 10. Tafel plots of electrodeposited catalysts (from literature data) and FeS nanoparticles (from this work) in water at pH 7.0. The Co/P/O curve (red) was recorded in a 0.5 mol/L phosphate buffer at 5 mV/s.[33] The curves for MoS_3 (blue), Fe−MoS_3 (green), Ni−MoS_3 (purple), and Co−MoS_3 (orange) were recorded in a phosphate buffer (unknown concentration) at 1 mV/s.[19] The curve for FeS nanoparticles (black) was recorded in a 0.1 mol/L phosphate buffer at 1 mV/s.

Table 2. Exchange Current Densities (J_0) of Different Electrocatalysts in Water at pH 7.0[a]

material	J_0 (mA cm^{-2})	slope (mV/dec)	η range (mV)	ref
Co−MoS_3	1.1 × 10^{-2}	87	87–122	19
Ni−MoS_3	1.0 × 10^{-2}	96	110–144	19
Fe−MoS_3	4.8 × 10^{-3}	95	137–176	19
Co/P/O	1.9 × 10^{-3}	134	200–300	33
MoS_3	8.9 × 10^{-4}	86	171–203	19
FeS	6.6 × 10^{-4}	150	350–450	this work

[a] Data were extracted from the polarization curves in Figure 10.

by about 300 mV relative to Co−MoS_3, the best in the molybdenum sulfide series reported by Hu and co-workers,[19] and by about 100 mV relative to the cobalt phosphate material reported by Artero and co-workers.[33]

3. SUMMARY AND CONCLUSIONS

We have demonstrated that a robust and efficient catalyst for molecular hydrogen evolution from neutral water that operates at a mild overpotential can be made from excessively cheap

dx.doi.org/10.1021/cs4011698 | ACS Catal. 2014, 4, 681–687

Earth-abundant materials and exhibits a catalytic activity exceeding 5 days.

Despite the fact that our FeS nanoparticles compare less favorably with cobalt phosphate or molybdenum sulfide materials at a given overpotential, the remarkable stability and the ease of preparation clearly show that the iron sulfide materials are very promising. If we now compare the abundance and cheapness of the different materials, the iron sulfide nanoparticles are clearly favored over cobalt phosphate or molybdenum sulfide materials. A rough comparison between the different metal prices shows that in 2012, iron ore ($101/ton) was much cheaper than nickel ($22,890/ton), molybdenum ($34,100/ton) or cobalt ($36,100/ton), with the platinum-group metals being much more expensive ($25,000,000/ton).[34] We can therefore envisage that iron sulfide nanoparticles may offer a great advantage in term of cost and availability compared with other transition-metal electrocatalysts for molecular hydrogen evolution, and further investigations on related materials are currently in progress.

4. EXPERIMENTAL SECTION

Methods and Materials. All of the chemicals were of analytical grade and were used without further purification. Octylamine and Nafion (0.05 thick membrane, perfluorosulfonic acid−PTFE copolymer, 5% w/w solution) were purchased from Alfa Aesar. Tetraethylammonium acetate and potassium phosphate were purchased from Sigma-Aldrich. The $Fe_2S_2(CO)_6$ precursor was synthesized according to previously published procedures.[29,30]

Instrumentation. XRD patterns were determined on a PANalytical X'Pert PRO diffractometer equipped with a multichannel X'Celerator detector using Co Kα radiation (λ = 1.7902) in the 2θ range 10−130°. The data were collected at room temperature with a step size of 0.033° and a time by step equal to 100 s. The refinement of the phase was determined using the MAUD software based on the Rietveld method combined with Fourier analysis,[35] which is well-adapted for nano-objects. The size of the coherent diffraction domains (crystallite size) was determined with both MAUD software and Highscore Plus software from PANalytical. Gas chromatography analyses for dihydrogen detection were performed on a Hewlett-Packard 6890 series GC system with a thermal conductivity detector fitted with a 2 m long Agilent Technology 1/8″ Carbosieve S3 60−80 mesh column and calibrated with pure H_2 gas.

Synthesis and Characterization of Nanoparticles. The synthesis of the particles was adapted from a published procedure.[36] In a typical synthesis, $Fe_2S_2(CO)_6$ (143 mg, 0.42 mmol) was dissolved in 35 mL of octylamine in a stainless steel autoclave equipped with a Teflon container at room temperature. The dark-red solution was placed in an oven at 230 °C and kept at this temperature overnight (ca. 16 h). The black precipitate obtained was centrifuged at 22 500 rpm in polypropylene copolymer tubes and washed five times with absolute ethanol, each washing being followed by centrifugation at 22 500 rpm. The collected black powder (62 mg, 0.70 mmol as FeS only, 84% yield), was dried under vacuum for 1 h at room temperature and then characterized as it was by XRD, EDX, TEM, SEM, and Mössbauer spectroscopy.

Microscopy. The particle size and morphology were determined by TEM and SEM. For TEM analysis, the powders were dispersed in chloroform, and a drop was placed on a 200 mesh carbon-coated copper grid. Images were recorded using a JEOL JEM-100CXII microscope operating at 100 kV. SEM images were obtained with a Zeiss Supra 40 scanning electron microscope. The images were taken at different magnifications using an In lens detector at a low voltage (5 kV) and in a small working distance (5 mm). An SEM image of a coated electrode was also taken. The atomic composition of the powder was analyzed using an EDX system with a JEOL 6510 scanning electron microscope. The analyses were performed at 15 kV and a work distance of 10 mm. The results were analyzed using the IRIDIUM Ultra software. The semiquantitative analyses (Table S1 in the Supporting Information) were obtained with a FeS_2 pyrite standard.

Mössbauer Spectroscopy. The ^{57}Fe Mössbauer spectra were recorded at 300 and 77 K with a bath cryostat in a transmission geometry using a ^{57}Co/Rh source mounted on a conventional electromagnetic drive with a triangular velocity form. The sample consisted of a thin powdered layer containing 5 mg of Fe/cm^2. The obtained Mössbauer spectra were analyzed by least-squares fitting to Lorentzian functions. The isomer shift values (δ) were referred to that of α-Fe at 300 K.

Electrochemistry. The potentiostat used for cyclic voltammetry was an Autolab PGSTAT 12. The working electrode was a 3 mm diameter glassy carbon (GC) rotating disk electrode (Tokai) that was carefully polished and ultrasonically rinsed in absolute ethanol before use. The counter electrode was a platinum wire, and the reference electrode was an aqueous SCE electrode. All of the potentials were referred to NHE by adding +0.244 V to the potential vs SCE (a conversion to RHE can be done by adding 0.059 × pH to the potential vs NHE). All of the experiments were carried out under argon at 20 °C at different scan rates and a rotation rate of 4000 rpm. From a mixture of pyrrhotite FeS nanoparticles (10 mg), Nafion (33 μL), and isopropanol (100 μL), 2 μL was deposited on the electrode surface, which was then dried in air and left for 12 h at 100 °C in an oven. A 0.1 mol/L phosphate buffer (pH 7.0) was prepared and used as a supporting electrolyte and degassed under argon. Experimental details for Figures 6, 7, 8, and 9 are detailed in the Supporting Information.

■ ASSOCIATED CONTENT

Ⓢ Supporting Information

Details of electrochemical measurements and additional nanoparticle characterizations. This material is available free of charge via the Internet at http://pubs.acs.org.

■ AUTHOR INFORMATION

Corresponding Authors

*E-mail: marion.giraud@univ-paris-diderot.fr.

*E-mail: cedric.tard@univ-paris-diderot.fr. Phone: +33 (0)157 278 783. Fax: +33 (0)157 278 787.

Notes

The authors declare no competing financial interest.

■ ACKNOWLEDGMENTS

The authors thank P. Beaunier, S. Drouet, M. Duca, M. Fournier, J.-Y Piquemal, and L. Sicard for experimental assistance. We also thank V. Ching, J. Peron, J.-Y. Piquemal, and M. Robert for helpful discussions and suggestions.

■ REFERENCES

(1) Bagotsky, V. S. *Fuel Cells: Problems and Solutions*, 2nd ed.; John Wiley & Sons: Hoboken, NJ, 2012.

(2) Armstrong, F. A.; Belsey, N. A.; Cracknell, J. A.; Goldet, G.; Parkin, A.; Reisner, E.; Vincent, K. A.; Wait, A. F. *Chem. Soc. Rev.* **2009**, *38*, 36−51.
(3) Frey, M. *ChemBioChem* **2002**, *3*, 153−160.
(4) Cracknell, J. A.; Vincent, K. A.; Armstrong, F. A. *Chem. Rev.* **2008**, *108*, 2439−2461.
(5) DuBois, D. L.; Bullock, R. M. *Eur. J. Inorg. Chem.* **2011**, 1017−1027.
(6) Tard, C.; Pickett, C. J. *Chem. Rev.* **2009**, *109*, 2245−2274.
(7) Yamamura, T.; Christou, G.; Holm, R. H. *Inorg. Chem.* **1983**, *22*, 939−949.
(8) Yuhas, B. D.; Smeigh, A. L.; Samuel, A. P. S.; Shim, Y.; Bag, S.; Douvalis, A. P.; Wasielewski, M. R.; Kanatzidis, M. G. *J. Am. Chem. Soc.* **2011**, *133*, 7252−7255.
(9) Yuhas, B. D.; Prasittichai, C.; Hupp, J. T.; Kanatzidis, M. G. *J. Am. Chem. Soc.* **2011**, *133*, 15854−15857.
(10) Yuhas, B. D.; Smeigh, A. L.; Douvalis, A. P.; Wasielewski, M. R.; Kanatzidis, M. G. *J. Am. Chem. Soc.* **2012**, *134*, 10353−10356.
(11) Thoi, V. S.; Sun, Y.; Long, J. R.; Chang, C. J. *Chem. Soc. Rev.* **2013**, *42*, 2388−2400.
(12) Karunadasa, H. I.; Chang, C. J.; Long, J. R. *Nature* **2010**, *464*, 1329−1333.
(13) Bigi, J. P.; Hanna, T. E.; Harman, W. H.; Chang, A.; Chang, C. J. *Chem. Commun.* **2010**, *46*, 958−960.
(14) Sun, Y.; Bigi, J. P.; Piro, N. A.; Tang, M. L.; Long, J. R.; Chang, C. J. *J. Am. Chem. Soc.* **2011**, *133*, 9212−9215.
(15) Andreiadis, E. S.; Jacques, P.-A.; Tran, P. D.; Leyris, A.; Chavarot-Kerlidou, M.; Jousselme, B.; Matheron, M.; Pécaut, J.; Palacin, S.; Fontecave, M.; Artero, V. *Nat. Chem.* **2013**, *5*, 48−53.
(16) Helm, M. L.; Stewart, M. P.; Bullock, R. M.; DuBois, M. R.; DuBois, D. L. *Science* **2011**, *333*, 863−866.
(17) Han, Z.; McNamara, W. R.; Eum, M.-S.; Holland, P. L.; Eisenberg, R. *Angew. Chem., Int. Ed.* **2012**, *51*, 1667−1670.
(18) Jaramillo, T. F.; Jørgensen, K. P.; Bonde, J.; Nielsen, J. H.; Horch, S.; Chorkendorff, I. *Science* **2007**, *317*, 100−102.
(19) Merki, D.; Vrubel, H.; Rovelli, L.; Fierro, S.; Hu, X. *Chem. Sci.* **2012**, *3*, 2515−2525.
(20) Merki, D.; Fierro, S.; Vrubel, H.; Hu, X. *Chem. Sci.* **2011**, *2*, 1262−1267.
(21) Karunadasa, H. I.; Montalvo, E.; Sun, Y.; Majda, M.; Long, J. R.; Chang, C. J. *Science* **2012**, *335*, 698−702.
(22) Vrubel, H.; Merki, D.; Hu, X. *Energy Environ. Sci.* **2012**, *5*, 6136−6144.
(23) McKone, J. R.; Sadtler, B. F.; Werlang, C. A.; Lewis, N. S.; Gray, H. B. *ACS Catal.* **2013**, *3*, 166−169.
(24) Chen, W.-F.; Sasaki, K.; Ma, C.; Frenkel, A. I.; Marinkovic, N.; Muckerman, J. T.; Zhu, Y.; Adzic, R. R. *Angew. Chem., Int. Ed.* **2012**, *51*, 6131−6135.
(25) Sun, Y.; Liu, C.; Grauer, D. C.; Yano, J.; Long, J. R.; Yang, P.; Chang, C. J. *J. Am. Chem. Soc.* **2013**, *135*, 17699−17702.
(26) Xu, Y.; Wu, R.; Zhang, J.; Shi, Y.; Zhang, B. *Chem. Commun.* **2013**, *49*, 6656−6658.
(27) Popczun, E. J.; McKone, J. R.; Read, C. G.; Biacchi, A. J.; Wiltrout, A. M.; Lewis, N. S.; Schaak, R. E. *J. Am. Chem. Soc.* **2013**, *135*, 9267−9270.
(28) Rickard, D.; Luther, G. W. *Chem. Rev.* **2007**, *107*, 514−562.
(29) Seyferth, D.; Henderson, R. S.; Song, L. C. *Organometallics* **1982**, *1*, 125−133.
(30) Stanley, J. L.; Rauchfuss, T. B.; Wilson, S. R. *Organometallics* **2007**, *26*, 1907−1911.
(31) Xu, F.; Navrotsky, A. *Am. Mineral.* **2010**, *95*, 717−723.
(32) Vandenberghe, R. E.; De Grave, E. In *Mössbauer Spectroscopy: Tutorial Book*; Yoshida, Y., Langouche, G., Eds.; Springer-Verlag: Berlin, 2013; pp 91−185.
(33) Cobo, S.; Heidkamp, J.; Jacques, P.-A.; Fize, J.; Fourmond, V.; Guetaz, L.; Jousselme, B.; Ivanova, V.; Dau, H.; Palacin, S.; Fontecave, M.; Artero, V. *Nat. Mater.* **2012**, *11*, 802−807.
(34) Kelly, T. D.; Matos, G. R. *Historical Statistics for Mineral and Material Commodities in the United States, 2012*; U.S. Geological Survey Data Series 140; http://minerals.usgs.gov/ds/2005/140/index.html.
(35) Lutterotti, L.; Matthies, S.; Wenk, H. R. *CPD Newsl.* **1999**, *21*, 14−15.
(36) Vanitha, P. V.; O'Brien, P. *J. Am. Chem. Soc.* **2008**, *130*, 17256−17257.